

Passive control of flow-excited acoustic resonance in rectangular cavities using upstream mounted blocks

Mahmoud Shaaban · Atef Mohany

Received: 2 September 2014 / Revised: 17 January 2015 / Accepted: 19 January 2015 / Published online: 21 March 2015
© Springer-Verlag Berlin Heidelberg 2015

Abstract A passive method for controlling the flow-excited acoustic resonance resulting from subsonic flows over rectangular cavities in channels is investigated. A cavity with length to depth ratio of $L/D = 1$ is tested in air flow of Mach number up to 0.45. When the acoustic resonance is excited, the sound pressure level in the cavity reaches 162 dB. Square blocks are attached to the surface of the channel and centred upstream of the cavity leading edge to suppress the flow-excited acoustic resonance in the cavity. Six blocks of different widths are tested at three different upstream distances. The results show that significant attenuation of up to 30 dB of the excited sound pressure level is achieved using a block with a width to height ratio of 3, while blocks that fill the whole width of the channel amplify the pressure of the excited acoustic resonance. Moreover, it is found that placing the block upstream of the cavity causes the onset of the acoustic resonance to occur at higher flow velocities. In order to investigate the nature of the interactions that lead to suppression of the acoustic resonance and to identify the changes in flow patterns due to the placement of the block, 2D measurements of turbulence intensity in the shear layer and the block wake region are performed. The location of the flow reattachment point downstream of the block relative to the shear layer separation point has

a major influence on the suppression level of the excited acoustic resonance. Furthermore, higher attenuation of noise is related to lower span-wise correlation of the shear-layer perturbation.

List of symbols

D	Cavity depth
d	Distance from cavity leading edge
f	Frequency
h	Block height
L	Cavity length
l	Characteristic shear-layer length
M	Mach number
P	Dynamic pressure
R	Correlation coefficient
Re	Reynolds number
St	Strouhal number
U	Flow velocity
u'	Velocity perturbation
W	Cavity width
w	Block width
x, y, z	Cartesian coordinates
α	Average convection speed
θ	Momentum thickness
κ	Phase delay
ρ	Density

Subscripts and superscripts

eff	Effective
∞	Inlet
r	Reduced
NB	No block
n, m	Mode number
re	Reattachment
*	Normalized

M. Shaaban (✉) · A. Mohany
Aeroacoustics and Noise Control Laboratory, Faculty
of Engineering and Applied Science, University of Ontario
Institute of Technology, Oshawa, ON, Canada
e-mail: mahmoud.shaaban@uoiit.ca

1 Introduction

Flow over cavities has been identified as a potential source of acoustic resonance in many engineering applications. The noise resulting from the resonance can be of high sound pressure levels and can result in structural failure. This problem has received attention after many related observations in aerodynamic applications. Krishnamurty (1955) and Rossiter (1962) noted the occurrence of such undesirable oscillations in high-velocity external flows of gases over cavities in aircraft surfaces. Lafon et al. (2003) and Ziada et al. (1989) studied the acoustic resonance resulting from flow over cavities and reported that the resulting dynamic loading and noise generation can be sufficiently high to pose structural and environmental hazard.

The reported oscillations are attributed to the inherent instability of the shear layer over a cavity which can give rise to pressure perturbation. Such perturbation can couple with a resonating acoustic field and engage in a feedback mechanism, resulting in sustained oscillations in the flow field. Rockwell (1983) classified the feedback mechanisms according to the nature of oscillations giving rise to them into: fluid-resonant, fluid-dynamic, and fluid-elastic oscillations. High oscillating pressure amplitudes are associated with the fluid-resonant feedback mechanism, in which the feedback effect is due to the fluctuations resulting from acoustic resonance. The fluid-resonant feedback cycle, illustrated in Fig. 1 is initiated when the shear layer over the cavity mouth starts to fluctuate at the cavity leading edge. Fluctuations are enhanced at frequencies that cause favourable phasing over the shear-layer length. The instability of the shear layer causes the perturbation to grow exponentially while they are convected downstream by the mean flow. Kang et al. (2008) suggested that turbulent boundary layer can give rise to the formation of large-scale vortical structures responsible for self-sustained oscillations. The vorticity field transfers energy to the acoustic field near the trailing cavity edge. The correct phasing between the consequent events at certain frequencies can excite the acoustic modes of the cavity to resonate. The cycle is then closed when the acoustic fluctuations at the leading edge are enhanced to develop vorticity perturbation (Rockwell and Naudascher 1978; Bian et al. 2011).

The interactions of the free shear layer with the acoustic field are amplified at frequencies defined by the semi-empirical formula developed by Rossiter (1964). The formula gives the Strouhal number as,

$$St_n = \frac{f_n l}{U_\infty} = \frac{n - \alpha}{M + \frac{1}{\kappa}}; \quad n = 1, 2, 3, \dots \quad (1)$$

where l is the characteristic shear-layer length, which is the distance the shear layer travels across the cavity until

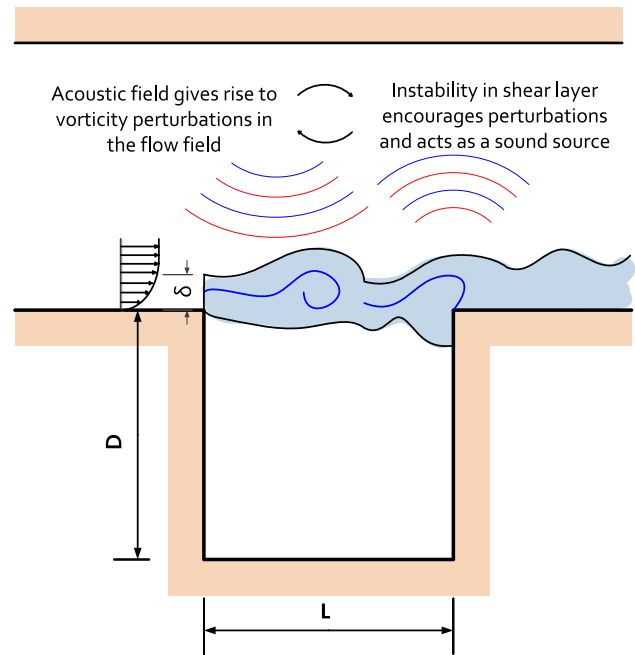


Fig. 1 Fluid-resonant feedback mechanism of the cavity flow oscillations

it reaches the trailing edge. St_n is the Strouhal number corresponding to the frequency f of the n th mode. κ and α are empirical constants that correspond to the average convection speed of the vortical disturbances in the shear layer and a phase delay, respectively. The value of $1/\kappa$ is typically 1.75 and α is typically equal to 0.25.

The perturbation of the flow particles in the shear layer is normal to the cavity mouth plane, making it able to provide energy to initiate a standing wave. At velocities where a shear-layer mode frequency coincides with one of the cross-modes, the phasing between the acoustic cycle and the shear-layer perturbation becomes favourable, and this lock-in increases the effectiveness of the feedback mechanism. This leads to an efficient conversion of dynamic energy into acoustic energy, which produces tonal pressure fluctuations of extremely high sound pressure levels. Ukeiley and Murray (2005) suggested that whether a cavity resonates or not may depend on the scale of the vorticity with respect to the impingement wall. Lafon et al. (2003) showed that the resonance modulation effect for the fluid resonance mechanism ensures that the acoustic modes are two-dimensional and the acoustic oscillation is in phase along the whole width. The oscillations produced by the separating shear layer over the cavity are influenced by the geometry of the separation and impingement points. Changes in the flow characteristics at the leading and trailing edges are reported to affect the sound pressure level (Rockwell and Naudascher 1978).

Several control techniques of flow-induced cavity oscillations are reviewed by Cattafesta et al. (2003) and Rowley and Williams (2006). They attributed the effect of acoustic resonance suppression of passive devices to one or more of the following three mechanisms: shifting the reattachment point downstream of the trailing edge, modifying the stability characteristics of the shear layer so that the resonant modes are not amplified, or disrupting the span-wise coherence of the shear layer. They also stated that many of these techniques require fine-tuning and can negatively affect off-design tone frequencies. McGrath and Shaw (1996) obtained a significant reduction in the sound pressure level (SPL) using an oscillating flab as a high-frequency tone generator just upstream of the cavity leading edge to manipulate the cavity shear layer and disrupt the feedback cycle. However, their results did not show the effect of the flab dimensions on the obtained attenuation. Sarno and Franke (1994) studied the use of fences at the upstream edge to suppress the flow-induced pressure oscillations in a cavity. They found that static fences are more suppressive than oscillating fences. However, the suppression effect is found to depend on the frequency mode and the flow Mach number. de Jong et al. (2011) found that rounding of the downstream edge reduces lock-on amplitude due to a reduction in flow entrainment into the cavity, thereby weakening the feedback cycle. Ukeiley et al. (2004) used a leading edge fence and a cylindrical rod at various locations to disturb the separation of the boundary layer. They showed that significant suppression can be obtained and noted that differences in the shear-layer lift over the impingement corner have an important effect on the level of the pressure attenuation. MacManus and Doran (2008) studied the effect of adding a span-wise step inside the cavity adjacent to the leading edge on attenuating the sound pressure level. They showed that an overall attenuation of 7.5 dB could be achieved and their flow visualization results showed that a large recirculation bubble exists on the top of the step face, resulting in an outward deflection of the shear layer. However, they did not investigate the influence of placing the step upstream of the leading edge. Moreover, the step size was fixed throughout their experiments.

A surface-mounted block in cross-flow is known to cause a complex pattern of vorticity which is convected to the downstream flow. Hussein and Martinuzzi (1996) experimentally studied the channel flow around square cross-sectional surface-mounted blocks. They found that the complex features of the flow are highly dependent on the aspect ratio of the block. Wider blocks cause higher turbulence intensity and longer wake region downstream. Hwang and Yang (2004) numerically investigated the vortical structures around a wall-mounted cubic obstacle in a channel flow. The simulations showed that the three-dimensional structures of the flow including separation,

entrainment regions, and reattachment arise as a result of the adverse pressure gradient induced by the obstacle geometry. Their simulation also showed that the increase in Reynolds number induces the generation of more complex aspects of the horseshoe vortex and the number of vortices increases in pairs. They also noted that the vorticity field near the cube is characterized by the generation of the hairpin vortices in the near-wake region at relatively low frequencies, and the shedding of lateral vortices from the leading lateral edges of the cubic obstacle. Hwang and Yang (2004) also highlighted the quasiperiodic behaviour of the hairpin vortices. The length and time scales of those vortices become smaller at higher Reynolds number. They also pointed out that the reattachment point is located at $x = 3h$, where x is the downstream distance measured from the downstream edge of the cube. It is important to note that the simulations of Hwang and Yang (2004) were limited to flows of Reynolds number as low as 3,500.

The use of the complex vortical structures observed behind rectangular surface-mounted obstacles to disturb the shear layer over the rectangular cavity mouth is a potential method to suppress the flow-induced acoustic resonance. The shear layer can be disturbed at the leading edge of the cavity with flow structures that are different in length and time scales than the shear-layer structures. Such disturbance can affect the phasing of events in the shear layer, decreasing the effectiveness of the fluid-resonant feedback mechanism that gives rise to noise of high sound pressure levels. Therefore, the objective of this study was to investigate the effect of placing square cross-sectional blocks of different widths at different locations upstream of the cavity leading edge on the mechanism of acoustic resonance excitation in a rectangular cavity with a flow of Mach numbers up to 0.45. The flow and acoustic measurements obtained are analysed to give better understanding of the flow-sound interactions which are responsible for favourable attenuation of the undesired resonance.

2 Experimental setup and procedure

The experiments were performed in an open-loop wind tunnel. A schematic representation of the test section is shown in Fig. 2. The cavity has a length of $L = 0.127$ m, a depth of $D = 0.127$ m, and a width of $W = 0.127$ m. The tunnel has a width of 0.127 m and a height of 0.254 m. The frequency of the first acoustic cross-mode is determined numerically as 482 Hz for a two-dimensional cavity with no-flow condition. This value is within 5 % of the experimentally measured frequency. The normalized acoustic pressure distribution for the first acoustic cross-mode is shown in Fig. 3. The inlet section of the apparatus is in the shape of a bellmouth to ensure uniform velocity

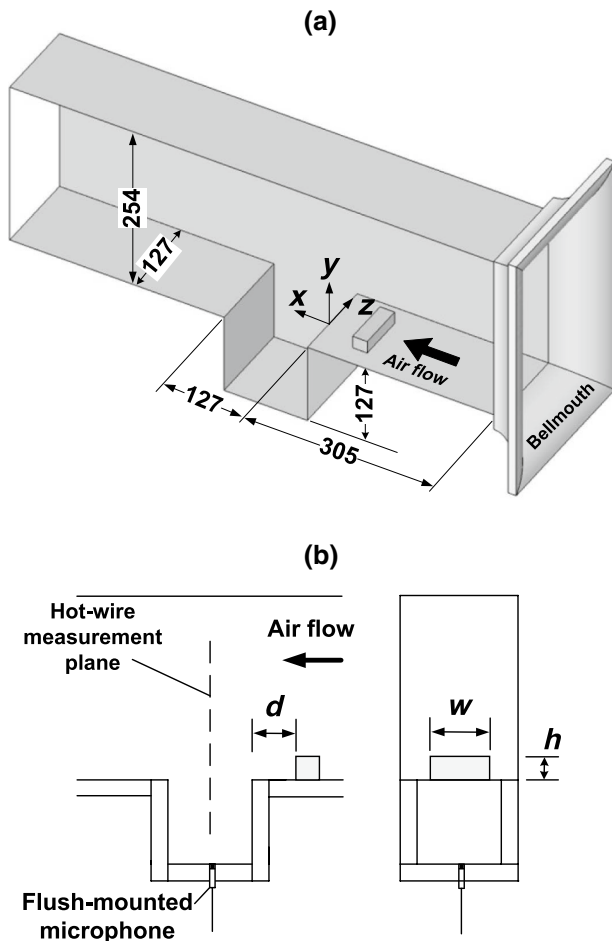


Fig. 2 **a** Dimensions, in mm, of the cavity test section with a block placed. **b** Nomenclature for the block configuration

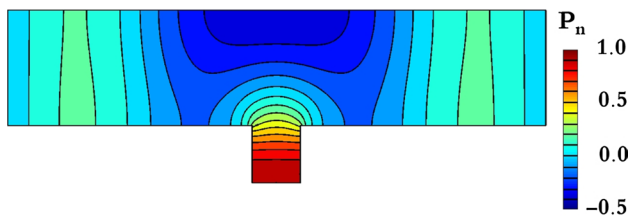


Fig. 3 Numerically calculated pressure amplitude distribution for the first acoustic cross-mode for a two-dimensional case, normalized by the maximum pressure value

profile within 1 % at the measurement section. The distance from the inlet edge to the cavity leading edge is 0.305 m. The test section includes the 0.127-m-long cavity followed by a 0.330-m-long rectangular tunnel section. A diffuser with a length of 0.625 m has the same tunnel height of 0.254 m, uniformly expanding in the width direction, reaching a width of 0.508 m at the blower inlet connection.

Six blocks of square cross section of edge length $h = 0.019$ m are tested, with width to height ratios $w/h = 1, 2, 3, 4, 5,$ and 6.66 . These blocks fill 15, 30, 45, 60, 75, and 100 % of the channel width. The last ratio is selected to fill the span-wise dimension of the tunnel cross section with no gaps at the sides to force the flow to pass over the block. The tested block is attached to the surface of the channel at a distance d upstream of the cavity leading edge. Three different distances were selected, $d/h = 0, 3,$ and 6 . These three locations are selected to cause the flow reattachment points to be approximately at $3h$ downstream of the cavity leading edge, at the cavity leading edge, and at $3h$ upstream of the cavity leading edge, respectively.

The air velocity is controlled through a variable frequency drive. The velocity of the air flow is increased from 0 up to 160 m/s. The attached block is rigidly mounted to prevent any vibrations. The pressure level is recorded using a $\frac{1}{4}$ -in. flush-mounted microphone located at the centre of the cavity bottom wall, which represents the location of the maximum acoustic pressure amplitude of the first acoustic cross-mode as shown in Fig. 3. The sampling rate is 10 kHz. The frequency spectra are calculated based on the averaging of 30 runs, each of 1 s duration to give the spectra extending up to 5 kHz with a resolution of 1 Hz.

Flow velocity perturbation, as an indication of the turbulence intensity, is measured using a model 55P16 CTA single hot-wire probe. Measurements for correlation are carried out using two similar hot-wire probes. The used sampling interval is 1 s, averaged on a 30-s period. A traverse mechanism is used to control the location of the probes with an accuracy of 1 mm in the coordinate system is shown in Fig. 2. The hot-wire measurements are carried out at non-resonant conditions. Measurements of the acoustic response of the cavity are always recorded in the absence of the hot-wire probe.

3 Base cavity response

The details of the acoustic response of the rectangular cavity with aspect ratio of $L/D = 1$ are discussed in this section to provide a base case on which the control effectiveness is assessed. The characteristics of the pressure perturbation in the cavity are described and the shear-layer modes that excite the resonant sound are identified.

The response of the system is characterized by the dimensionless pressure P^* , defined by Eq. 2.

$$P^* = \frac{P}{0.5\rho U_\infty^2} \quad (2)$$

where P is the pressure amplitude, ρ and U_∞ are the free-stream flow density and velocity, respectively. The values of P^* reported in the literature vary according to the scale

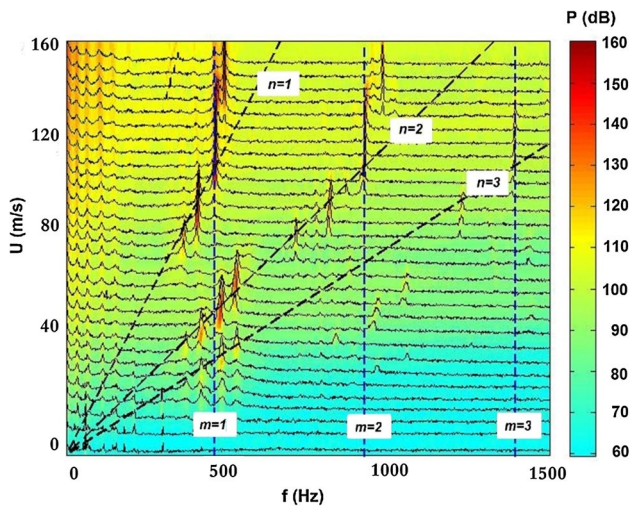


Fig. 4 Acoustic response of the cavity for increasing air velocity with no block placed

of the cavity and the range of flow Mach number. Ziada and Shine (1999) reported values of $P^* = 10$ for coaxial branches at Reynolds number of 0.5×10^6 . Rockwell et al. (2003) reported values of $P^* = 0.6$ for sufficiently deep cavities with minimum damping, dropping to $P^* = 0.04$ for shallower cavities in a system with high damping. The flow velocity is indicated in the reduced form U_r , based on the frequency of the lowest acoustic cross-mode of the test section f_1 , as shown in Eq. 3.

$$U_r = \frac{U_\infty}{f_1 l} \tag{3}$$

Figure 4 shows the pressure spectra of the cavity measured at discrete values of flow velocities using the microphone which is flush-mounted at the centre of the cavity bottom wall. The spectral lines in the figure are obtained by applying a fast Fourier transform on the recorded data for each flow velocity, giving the acoustic pressure response of the cavity at velocities from $U_\infty = 0$ to 160 m/s.

Figure 4 shows that three distinct shear-layer modes are responsible for the excitation of tonal noise. The three modes, referring to $n = 1, 2,$ and 3 in Eq. 1, are theoretically depicted as three dashed lines starting at origin in Fig. 4. At the coincidence of a certain shear-layer mode with any of the resonant acoustic modes, $m = 1, 2,$ or 3 , a look-in region in which a tonal sound of constant frequency dominates. The three first acoustic cross-modes occur at frequencies $f_1 = 482$ Hz for $m = 1, f_2 = 946$ Hz for $m = 2,$ and $f_3 = 1,355$ Hz for $m = 3$. The deviation of the first acoustic cross-mode frequency from the calculated value of 482 Hz is attributed to the fact that the acoustic mode is calculated for the no-flow condition. Increase in flow velocities is expected to change the convection velocity, which

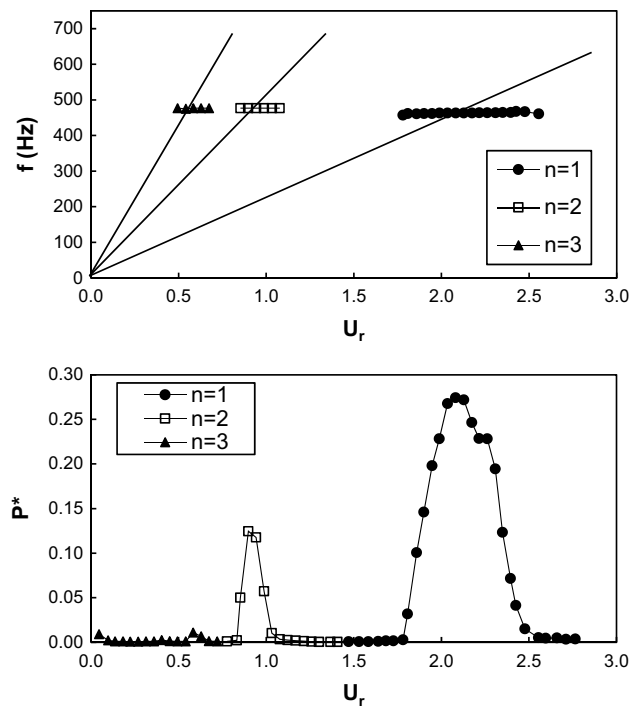


Fig. 5 Frequency of the resonant peaks and development of the normalized acoustic pressure with increasing reduced flow velocity in the rectangular cavity with no block placed

in turn will affect the resonance frequency. In addition, the effect of the fluid added mass is expected to change the theoretically calculated resonance frequency, as discussed by Mohany and Ziada (2009, 2011). Due to the relatively high amplitude of the first acoustic cross-mode at resonance, it is referred to as the resonant cross-mode in the following discussions.

Figure 5 shows the frequency and the dimensionless acoustic pressure P^* of the peaks at the resonant cross-mode with increasing reduced flow velocities. The frequency at resonance ranged between 463 and 469 Hz in the range of Mach number up to 0.45, which deviates by less than 5 % of the numerically calculated value of 482 Hz for the mode shown in Fig. 3. Figure 5 also shows the frequency at which resonance is detected with increasing reduced velocities. The frequency of the third shear-layer mode coincides with the frequency of the first acoustic cross-mode in the reduced velocity range between 0.51 and 0.64. The relatively low velocity, combined with the higher energy needed to sustain the third shear-layer mode provides low energy for the excitation and results in weak oscillations of $P^* = 0.01$ at a sound pressure level of SPL = 112 dB. At reduced velocities ranging from 0.83 to 1.06, the look-in between the second shear-layer mode and the first resonant cross-mode occurs, and a sound pressure level of SPL = 141 dB, corresponding to $P^* = 0.12$ is

measured. A wider look-in region dominates at the coincidence of the first shear-layer mode and the first acoustic cross-mode in the reduced velocity range between 1.75 and 2.53. The dynamic pressure in this region reaches $P^* = 0.27$ which corresponds to $\text{SPL} = 162$ dB.

The peaks of the dimensionless pressure occur at the frequency coincidence of the shear-layer modes and the acoustic cross-modes. The first cross-mode with $f_1 = 465$ Hz peaks at Strouhal number $St = 0.48, 1.11,$ and 1.61 referring to coincidence with the first, second, and third shear-layer mode frequencies, respectively. The values of normalized pressure amplitude and normalized frequency are consistent with the values reported in the literature (e.g. Aly and Ziada 2010; Rockwell et al. 2003).

4 Controlled cavity response

The acute tonal resonance produced by the rectangular cavity in Sect. 3 reached levels that are intolerable in many environments with the sound pressure level reaching 162 dB. The suggested passive control method aims to limit the high sound pressure level of the resonant mode. The objective of this section is to study the effectiveness of the block configuration in suppressing acoustic resonance in rectangular cavities. The spectral characteristics of the acoustic response with the block placed are also discussed.

The configuration of the block used to control the cavity flow-excited acoustic resonance determines the level of acoustic pressure attenuation that can be achieved. Figure 6 shows the development of the sound pressure level of the resonant acoustic cross-mode measured for different block configurations and locations. A notable observation is that the peak pressure occurs at a higher flow velocity when the block is placed. The significant influence of the block on the sound pressure level is clearly shown by the shift of the reduced velocity at which the peak value of pressure prevails. When the block fills the whole channel width, the look-in region is shifted to peak nearly at $U_r = 3.10$. This shift is related to the change in the Strouhal number at which the coincidence between the shear-layer mode and resonant acoustic cross-mode is expected to take place, which is believed to be related to a change in the shear-layer effective length due to changes in the path which the air flow has to take around the block.

When the block is placed at $d/h = 3$, the pressure amplitude of the resonance is highly suppressed. For each width, the peak pressure has a lower value at $d/h = 3$ than that at $d/h = 0$ or 6. The width ratio of $w/h = 1$ causes a resonance with a pressure amplitude of $P = 1,280$ Pa, while the placement of the block with width ratio of $w/h = 6.66$

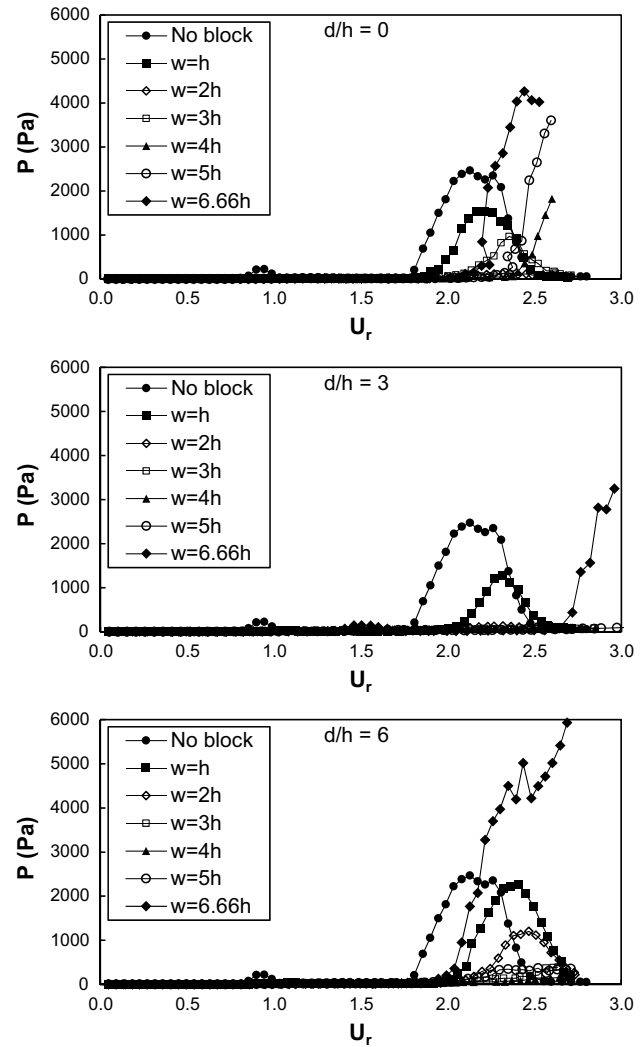


Fig. 6 Development of the sound pressure level of the resonant acoustic cross-mode with reduced velocity for different block configurations attached upstream of the cavity

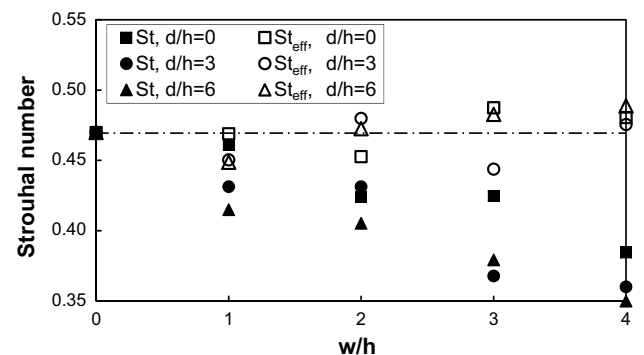


Fig. 7 Strouhal numbers at the highest values of sound pressure level at resonance for different block widths and locations, St for solid symbols and St_{eff} for open symbols

is responsible for a pressure amplitude of $P = 3,556$ Pa, which corresponds to a pressure amplification of 3.26 dB from the base case.

4.1 Strouhal number

Figure 7 shows the values of the Strouhal number at the acoustic pressure peak for the cavity with blocks at the three distances and for w/h up to 4. As defined in Eq. 1, the value of Strouhal number is calculated with the base shear-layer length l used as the characteristic length.

The occurrence of the coincidence at higher velocities suggests that the shear-layer mode has lower values of Strouhal number $St = f_1 l / U_\infty$ based on the base cavity length l . Noting that the frequency of the first acoustic cross-mode is not significantly affected by the presence of the cavity walls for block widths up to $w/h = 4$, the shift in the Strouhal number St is attributed to a change in the characteristic shear-layer length due to the change in the flow path around the block. This effective parameter has a clear dependency on w/h and d/h . The relationship is investigated by fitting the measured data to satisfy the condition that $St_{\text{eff}} = f_1 l_{\text{eff}} / U_\infty \simeq St_{\text{NB}}$. This data are fitted to the form of $l_{\text{eff}} = (c_1 * l^2 + (c_2 * d + c_3 * w)^2)^{0.5}$. This form is selected as the effective length is interpreted in two orthogonal components to account for the diverging direction of the flow in the wake of the block. The components are the direct path between the leading and trailing cavity edges, l , and the span-wise component which is dependent upon the configuration of the block. The effective shear-layer length that fits the data is given by the following equation

$$l_{\text{eff}} = \sqrt{l^2 + \left(\frac{d}{4} + \frac{5w}{4}\right)^2} \tag{4}$$

The values of the effective Strouhal number St_{eff} are shown in Fig. 7. Using values of St_{eff} , the highest values of the sound pressure level occur at values of St_{eff} within $\pm 5\%$ of the base St_{NB} , as shown in Fig. 8.

4.2 Attenuation of acoustic pressure

The placement of blocks at the upstream edge has a significant effect on the acoustic pressure level produced by the cavity. Figure 9 shows the attenuation of the sound pressure level due to the placement of blocks with different widths at different distances from the cavity upstream edge. Placing the cubic block, which fills 15% of the channel width, induces attenuation of less than 8 dB for all edge distances. The use of blocks with moderate widths leads to substantial

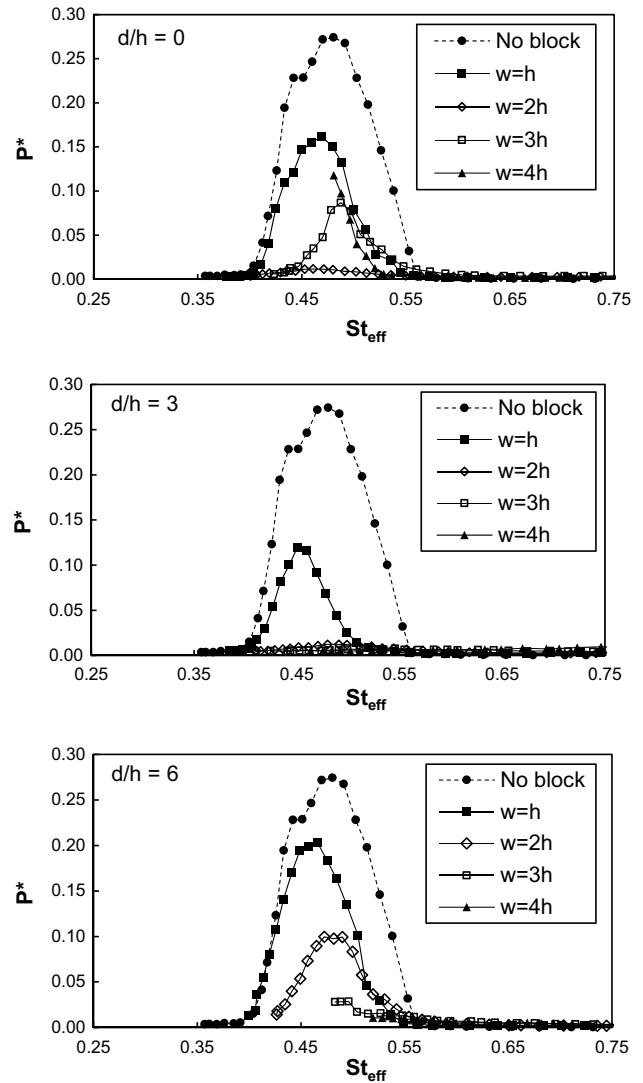


Fig. 8 Dimensionless acoustic pressure dependency on the block configuration and effective Strouhal number

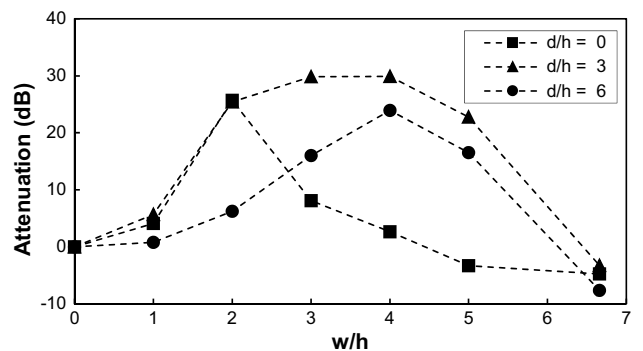


Fig. 9 Attenuation of the cavity acoustic pressure due to placement of blocks of different configurations

improvement in the attenuation levels. Blocks placed at a distance of $3h$ from the edge cause a significant level of attenuation reaching around 30 dB over a range of widths between $w/h = 2$ to 5, which is equivalent to 30–75 % of the channel width. The other edge distances show lower attenuation levels. The blocks placed at the edge cause a maximum attenuation of 26 dB for blocks of width $w/h = 2$, while blocks placed at $d/h = 6$ away from the cavity leading edge cause a maximum attenuation of 23 dB at $w/h = 4$.

It is important to note that the placement of blocks that filled the whole channel width at the three distances do not suppress the acoustic pressure, but amplify it instead as indicated by the negative attenuation values. This behaviour indicates that the existence of the horseshoe vortices shed at the block vertical upstream sides has an essential contribution to the suppression mechanism. This behaviour can also be related to the disturbance of the span-wise coherence of the shear layer due to the placement of the block.

4.3 Interactions at the leading edge

The feedback mechanism that leads to the high sound pressure levels at resonance is associated with the organized structures of the shear layer when it separates at the leading edge. The control effect of the blocks is related to the interactions of the lateral vortical formations in the wake of the block with the shear layer, disturbing its span-wise coherence. It is noteworthy to investigate the effect of the flow reattachment distance of the vortices forming at the sides of the block on the attenuation of the excited sound pressure level. Martinuzzi and Tropea (1993) described a linear relationship between the width to edge height ratio of the block and the distance of reattachment of the lateral horseshoe vortices in the range of w/h up to 8. They concluded that at high Reynolds numbers, the reattachment point occurs at a distance x_{re} from the block downstream surface, calculated as

$$x_{re} = 0.681w + h \quad (5)$$

The distance d_{re} of the block-side wake reattachment point measured from the leading edge. It is positive for cases where the reattachment point is downstream of the leading edge and negative if it is upstream of the leading edge. d_{re} is obtained as

$$d_{re} = x_{re} - d \quad (6)$$

Figure 10 shows the effect of the distance between the reattachment points from the cavity leading edge normalized by the block height, d_{re}/h , on the obtained attenuation of the excited acoustic resonance. The results with blocks of width ratio $w/h = 6.66$ are not shown in this graph as

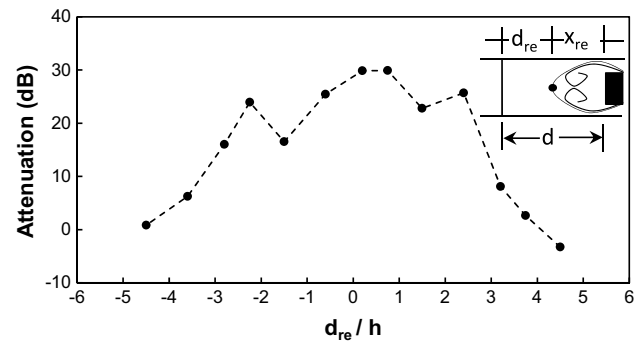


Fig. 10 Effect of the flow reattachment point downstream of the block on the attenuation of the excited acoustic pressure in the cavity

they do not produce lateral vortices. Blocks that cause the flow to reattach closer to the leading edge are more effective than cases where the reattachment of the block-side wake occurs either upstream or downstream from the cavity edge. The reattachment point defines a region of confined flow adjacent to the block downstream and side faces, inducing a region of highly reduced, and at some locations reversed, flow velocities. If the reattachment of the flow occurs closer to the cavity leading edge, the vortical structures in the wake of the block can disrupt the formation of vortices at the cavity mouth with higher efficiency, decreasing the effectiveness of the feedback mechanism that transfers energy from the flow field to the acoustic field to sustain the acoustic resonance.

5 Flow characteristics over the cavity

The results in Sect. 4 show that the introduction of the block upstream of the cavity has favourable effects on the flow–sound interactions leading to suppression of acoustic resonance. The location of the reattachment point of the block-side wake with respect to the leading edge plays a vital role in the mechanism as suggested by the behaviour shown in Fig. 10. The formation of vortices on the side edges of the block causes favourable interactions with the shear layer over the cavity mouth, which in turn provides a suppression effect that is absent in cases with no block-side flow. The effect can also be related to the changes in the coherence of the shear-layer periodicities when blocks separate the leading edge into distinct regions.

Figure 11 shows the vertical profiles of the normalized mean flow velocity and normalized root mean square of the perturbation in the shear layer for the base cavity case with no upstream blocks. The vertical profiles measured at the leading edge, $x = 0.0$ and at the middle plane, $x = L/2$ for $U_\infty = 2.5$ m/s. The measurements are done at the span-wise centre, $z = 0$. The figures show the growth of the

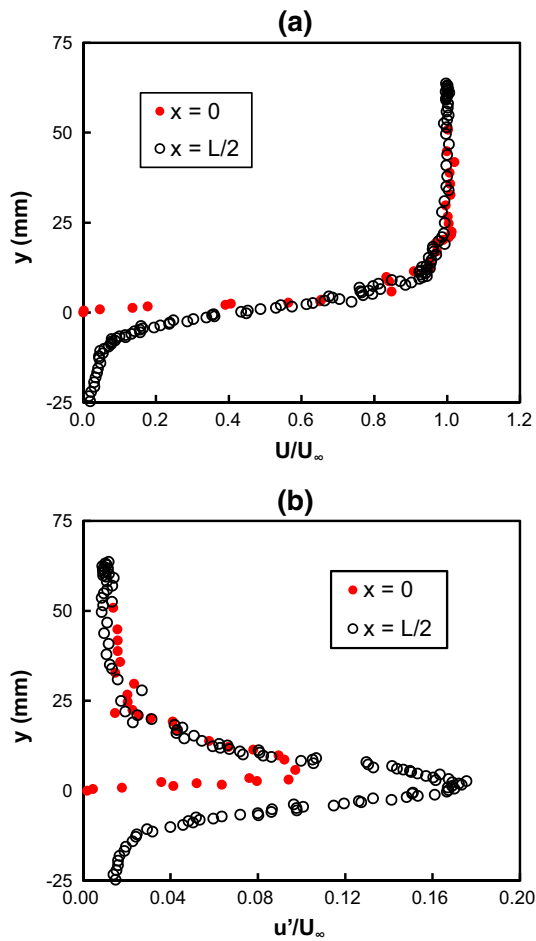


Fig. 11 **a** Normalized mean velocity and **b** normalized RMS of the perturbation in the shear layer at the leading edge ($x = 0$) and at the middle of the cavity ($x = L/2$) for $U_\infty = 2.5$ m/s

shear layer as it extends over the cavity. The profiles also show the increasing magnitude of perturbation as the shear layer grows.

Figure 12 shows the relationship between the measured boundary layer momentum thickness, θ , and the free-stream mean velocity at the leading edge for the base cavity case with no upstream blocks. The momentum thickness of the turbulent boundary layer is assumed to follow a power law where $\theta/x \sim Re_x^{-0.2}$. The boundary layer momentum thickness in Fig. 12 is measured at flow velocities between 2.3 and 20 m/s to avoid measurements in resonant conditions. At higher air velocities at which resonance may occur, the block dimensions are significantly larger than the momentum thickness, which indicates that the whole thickness of the shear layer is affected by placing the blocks at three distances from the cavity leading edge.

In order to investigate the shear-layer flow characteristics, measurements of the turbulence intensity are carried out in the mid-plane of the cavity, $x = 0.0635$ m

perpendicular to the flow direction at a constant inlet velocity of $U_\infty = 35$ m/s. Changes in flow regions of high turbulence are indication of the behaviour of the shear layer in response to changes in the configuration of the placed block. Flow patterns have been investigated for the cases with no blocks and with blocks of $w/h = 1, 3,$ and 6.66 at the three normalized distances from the cavity leading edge; 0, 3, and 6.

Figure 13 shows contours of the turbulence intensity u'/U_∞ for the base case at $U_\infty = 20$ m/s. The figure shows that the flow at that plane, at which the microphone is located, is almost two-dimensional. The white solid lines show the projected location of the leading edge of the cavity. The shear layer at the plane of measurement extends over a thickness of $0.9h$. The turbulence intensity is the

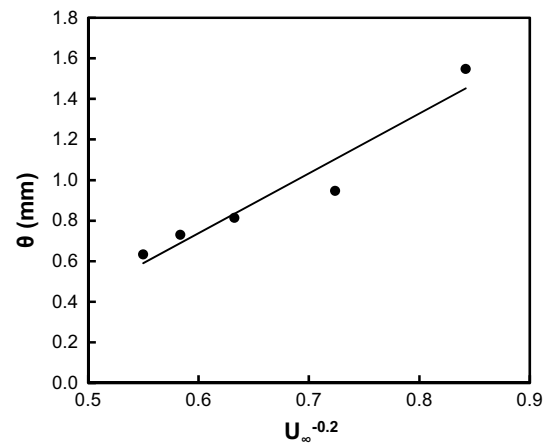


Fig. 12 Boundary layer momentum thickness at the leading edge

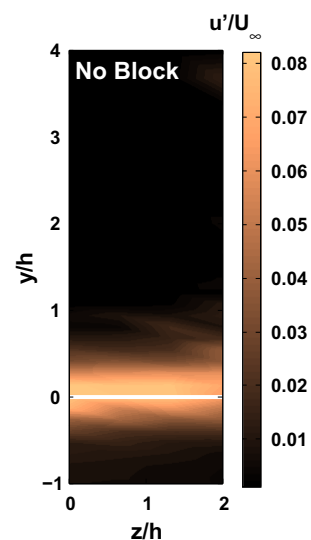


Fig. 13 Contours of turbulence intensity at $x = 0.0635$ m with no blocks placed

highest at $y/h = 0$. A region of high turbulence extends between $y/h = -0.5$ and 0.5 . No significant edge effects are detected at the measurement region that extends to $z/h = 2$, with the walls at $z/h = 3.33$.

The placement of the blocks has major effects on the structure of the shear layer as can be clearly seen in Fig. 14. The placement of the blocks of width $w/h = 1$ deforms the shear layer size and shape. When the block is placed at the edge, the shear layer extends to different heights at different values of the lateral position. For the case with the cubic block placed at $d/h = 3$ and 6 upstream of the cavity leading edge, it can be seen that the shear layer is deformed and extends to different thickness at different lateral locations, with a less centralized distribution for the latter case.

The contour plots in the second row of Fig. 14 show the velocity fluctuation pattern at the mid-plane of the cavity when blocks of $w/h = 3$ are placed upstream. These configurations show effectiveness in attenuating the sound pressure level. The placement of the block at the edge causes a large region of high turbulence intensity that reaches $y/h = 2.8$. The two other distances, $d/h = 3$ and 6 , have less distorted form of the shear layer.

The blocks of width $w/h = 6.66$ have a negative effect on acoustic pressure attenuation. More acute noise and higher sound pressure levels are detected when these blocks filled the whole cross section of the wind tunnel. It can be seen from the lowest row of Fig. 14 that a uniform thickness of the shear layer prevails in the whole measurement plane. The introduction of the blocks lifts the shear layer vertically to $y/h = 2$, as indicated by the symmetry of the turbulence intensity value around this height. However, this lift of the shear layer is not associated with a suppression effect at resonance.

In order to investigate the influence of the block attachment on the correlation of the flow in the shear layer, the coefficient of the cross-correlation between shear-layer perturbation at a reference point and at other points in the span-wise direction is calculated as,

$$R_{u'u'_0} = \frac{u'(z_0) \star u'(z)}{\sqrt{u'(z_0) \star u'(z_0)} \sqrt{u'(z) \star u'(z)}} \quad (7)$$

where the star \star refers to spatial cross-correlation, $u'(z_0)$ refers to shear-layer perturbation at the reference point at $z = 0$, and $u'(z)$ is the perturbation at the other measurement point. The blocks are attached at $d/h = 3$. The perturbation magnitude is evaluated at the line $x = L/2$ and $y = -0.013$ m. This span-wise line is at the edge of the shear layer inside the cavity as seen in Fig. 11, where the

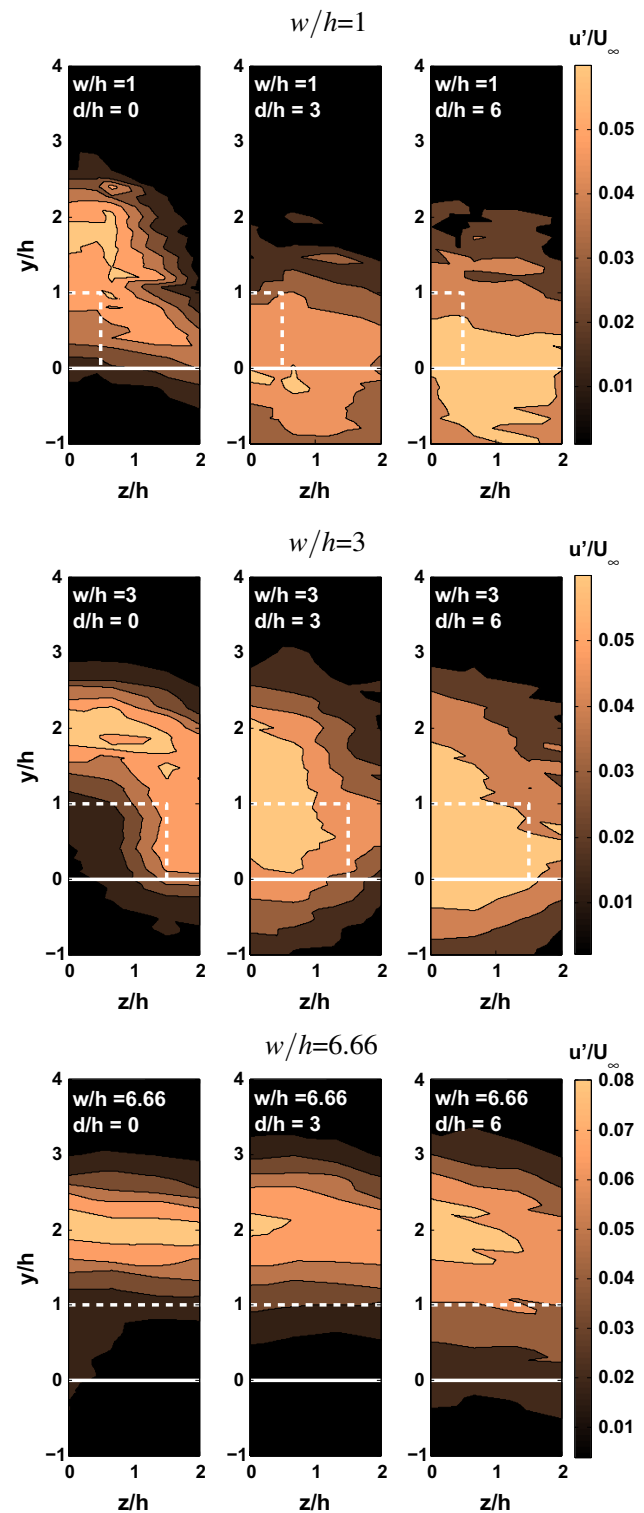


Fig. 14 Contours of turbulence intensity at the cavity mid-plane, $x = 0.0635$ m, for blocks with $w/h = 1, 3$, and 6.66 located at different upstream distances $d/h = 0, 3$, and 6

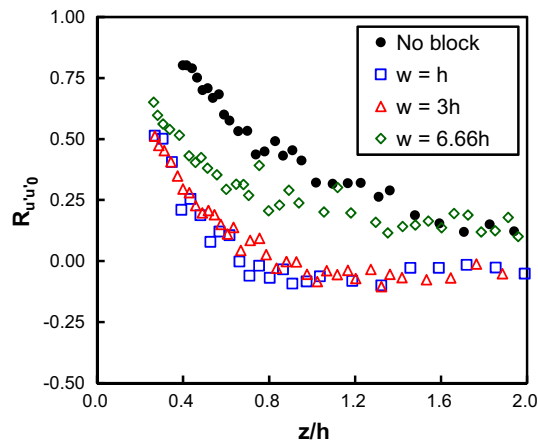


Fig. 15 Correlation coefficient of the shear-layer perturbation in the span-wise line ($x = L/2$, $y = -0.13$ m, z) for $U_\infty = 2.5$ m/s. The blocks are attached at $d = 3h$

shear-layer perturbation is distinguishable from perturbation due to turbulence. The coefficient of correlation, $R_{u'u'_0}$ of the flow perturbation, is shown in Fig. 15.

When no block is attached, the correlation coefficient is higher than the cases where a block is attached. The block filling the cavity, which did not attenuate the resonance, has lower correlation coefficient at values of z/h up to 1.5, and then it approaches the same value of 0.2 as the no-block case. When a block of smaller width is attached at $d/h = 3$, the correlation coefficient decreases at closer span-wise positions and reaches $R_{u'u'_0} = 0.0$ at $z/h = 0.8$ and then approaches a value of -0.1 . This shows that the block attenuation effect is related to lower correlation of the shear layer in the span-wise direction.

From this discussion, it is useful to develop a description of the flow features downstream of the blocks. The measurements indicate that blocks of intermediate width, filling 45 % of the channel width, develop a less-uniform shear layer that extends to further distances downstream of the blocks. When the blocks are placed at the edge, the turbulent region is lifted over the cavity mouth. On the other hand, the placement of the blocks at further distance from the cavity upstream edge causes higher turbulence inside the cavity. The existence of a region of high turbulence adjacent to the side of the block indicates that the turbulent flow structures that form at the sides of the block affect the span-wise flow coherence, which has an important contribution to the attenuation of the excited acoustic pressure. If the block fills the whole channel width, higher acoustic pressure is measured at resonance, and a thicker shear layer is observed. The hot-wire measurements presented in this section provide some insight into the complex flow characteristics around the blocks and its interaction with the cavity shear layer. However, phase-locked PIV measurements

during acoustic resonance can further clarify the role of the horseshoe vortical structure on the suppression mechanism of the acoustic resonance.

6 Conclusion

In this paper, a passive method for controlling the flow-excited acoustic resonance resulting from subsonic flows over rectangular cavities in channels is investigated. A cavity of width, length, and depth of 0.127 m is tested in air flow of Mach number up to 0.45. The resonance of the first acoustic cross-mode results in high sound pressure level of 162 dB when excited by the first shear-layer mode.

The placement of a solid square cross-sectional block centred on the channel surface upstream of the cavity leading edge is investigated as a way to suppress the flow-excited acoustic resonance. In order to evaluate their acoustic pressure attenuation effect, blocks of the same height of $h = 0.019$ m and of six different width to height ratios are tested. Each block is placed at three different locations upstream of the cavity leading edge. The highest attenuation, referred to the base case, reached 30 dB and is achieved by attaching the block of $w/h = 3$ at a distance of $d/h = 3$. The sound pressure level at the first acoustic resonance mode is attenuated by more than 25 dB using blocks of widths w/h between 2 and 4, which fills 30–60 % of the width of the channel. The placement of each block at a distance $d/h = 3$ upstream of the cavity leading edge is more effective than placing it at $d/h = 0$ or 6. Blocks that fill 100 % of the channel width amplify the acoustic pressure level when attached at any of the three distances. Higher attenuation is obtained when the reattachment of the block wake occurs closer to the cavity leading edge. Moreover, placing the blocks is found to shift the resonance of the first acoustic cross-mode to occur at higher flow velocities at the same frequency, which is related to a change in the effective shear-layer length due to the introduction of the block. Therefore, a formula is introduced to relate the effective shear-layer length to the block dimensions.

The hot-wire measurements reveal that the introduction of the blocks significantly affects the flow pattern in the shear layer over the cavity mouth. Significant attenuation of the resonance pressure level is associated with high turbulence levels at the sides of the block, indicating that the vortices shed at the sides of the block disturb the span-wise flow coherence and interact with the shear layer at the cavity leading edge. When a block filling 100 % of the channel width is attached, the shear layer is thicker than the base case and is uniform in the span-wise direction. The cases that did not attenuate the noise also has higher correlation coefficient between the perturbation in at the shear-layer

edge in the span-wise direction than cases that cause high attenuation of the excited sound pressure level.

Acknowledgments The authors thankfully acknowledge the financial support provided by the Natural Sciences and Engineering Research Council of Canada (NSERC).

References

- Aly K, Ziada S (2010) Flow-excited resonance of trapped modes of ducted shallow cavities. *J Fluids Struct* 26(1):92–120
- Bian S, Driscoll JF, Elbing BR, Ceccio SL (2011) Time resolved flow-field measurements of a turbulent mixing layer over a rectangular cavity. *Exp Fluids* 51(1):51–63
- Cattafesta L, Williams D, Rowley C, Alvi F (2003) Review of active control of flow-induced cavity resonance. In: AIAA paper 3567
- de Jong AT, Bijl H, Scarano F (2011) The aero-acoustic resonance behavior of partially covered slender cavities. *Exp Fluids* 51(5):1353–1367
- Hussein H, Martinuzzi R (1996) Energy balance for turbulent flow around a surface mounted cube placed in a channel. *Phys Fluids* 8(3):764–780
- Hwang JY, Yang KS (2004) Numerical study of vortical structures around a wall-mounted cubic obstacle in channel flow. *Phys Fluids* 16(7):2382–2394
- Kang W, Lee SB, Sung HJ (2008) Self-sustained oscillations of turbulent flows over an open cavity. *Exp Fluids* 45(4):693–702
- Krishnamurthy K (1955) Acoustic radiation from two-dimensional rectangular cutouts in aerodynamic surfaces. NACA technical note 3487. National Advisory Committee for Aeronautics, Washington, DC
- Lafon P, Caillaud S, Devos J, Lambert C (2003) Aeroacoustical coupling in a ducted shallow cavity and fluid/structure effects on a steam line. *J Fluids Struct* 18(6):695–713
- MacManus DG, Doran DS (2008) Passive control of transonic cavity flow. *J Fluids Eng* 130(6):064–501
- Martinuzzi R, Tropea C (1993) The flow around surface-mounted, prismatic obstacles placed in a fully developed channel flow. *J Fluids Eng* 115(1):85–92
- McGrath S, Shaw L (1996) Active control of shallow cavity acoustic resonance. In: AIAA paper 1949
- Mohany A, Ziada S (2009) Effect of acoustic resonance on the dynamic lift forces acting on two tandem cylinders in cross-flow. *J Fluids Struct* 25(3):461–478
- Mohany A, Ziada S (2011) Measurements of the dynamic lift force acting on a circular cylinder in cross-flow and exposed to acoustic resonance. *J Fluids Struct* 27(8):1149–1164
- Rockwell D (1983) Oscillations of impinging shear layers. *AIAA J* 21(5):645–664
- Rockwell D, Naudascher E (1978) Review: self-sustaining oscillations of flow past cavities. *J Fluids Eng* 100(2):152–165
- Rockwell D, Lin JC, Oshkai P, Reiss M, Pollack M (2003) Shallow cavity flow tone experiments: onset of locked-on states. *J Fluids Struct* 17(3):381–414
- Rossiter J (1962) The effect of cavities on the buffeting of aircraft. Royal Aircraft Establishment technical memorandum 754
- Rossiter J (1964) Wind-tunnel experiments on the flow over rectangular cavities at subsonic and transonic speeds. Ministry of Aviation, Royal Aircraft Establishment, RAE Farnborough
- Rowley CW, Williams DR (2006) Dynamics and control of high-Reynolds-number flow over open cavities. *Annu Rev Fluid Mech* 38:251–276
- Sarno R, Franke M (1994) Suppression of flow-induced pressure oscillations in cavities. *J Aircr* 31(1):90–96
- Ukeiley L, Murray N (2005) Velocity and surface pressure measurements in an open cavity. *Exp Fluids* 38(5):656–671
- Ukeiley LS, Ponton MK, Seiner JM, Jansen B (2004) Suppression of pressure loads in cavity flows. *AIAA J* 42(1):70–79
- Ziada S, Shine S (1999) Strouhal numbers of flow-excited acoustic resonance of closed side branches. *J Fluids Struct* 13(1):127–142
- Ziada S, Buehlmann E, Bolleter U (1989) Flow impingement as an excitation source in control valves. *J Fluids Struct* 3(5):529–549